Study of two-dimensional electron systems in the renormalized-ring-diagram approximation

Xin-Zhong Yan[1,2] and C. S. Ting[1]
[1]*Texas Center for Superconductivity, University of Houston, Houston, Texas 77204, USA*
[2]*Institute of Physics, Chinese Academy of Sciences, P.O. Box 603, Beijing 100080, China*
(Received 11 October 2006; revised manuscript received 12 January 2007; published 31 January 2007)

With a superhigh-efficiency numerical algorithm, we are able to self-consistently calculate Green's function in the renormalized-ring-diagram approximation for a two-dimensional electron system with long-range Coulomb interactions. The obtained ground-state energy is found to be in excellent agreement with that of the Monte Carlo simulation. The numerical results of the self-energy, the effective mass, the distribution function, and the renormalization factor of Green's function for the coupling constants in the range $0 \leqslant r_s \leqslant 30$ are also presented.

DOI: 10.1103/PhysRevB.75.035342 PACS number(s): 73.20.Mf, 71.10.Ca, 02.70.Hm, 71.18.+y

I. INTRODUCTION

Two-dimensional electron systems (2DESs) with long-range Coulomb interactions, realized in the semiconductor heterostructures and inversion layers,[1] continuously attract a lot of attention despite the fact that it has been studied for more than three decades. Most of the theoretical calculations so far were based on the random-phase approximation (RPA),[2–5] which is expected to be accurate in the weak-coupling or high-density regime. For taking into account the strong-coupling effect beyond the RPA, the usual way is to adopt the local-field correction (LFC) to the RPA.[6–11] In all these works, the Green's functions that appeared in the diagrams of the standard RPA as well as the one with the LFC are not renormalized. A crucial condition for a better approximation is that the renormalized Green's function should satisfy some microscopic conservation laws; otherwise, the approximation may lead to unphysical consequences.[12] Among various approximations, the renormalized-ring-diagram approximation (RRDA), in which Green's function needs to be self-consistently determined from the relevant integral equations, is well known to satisfy this condition[12] and thus should be a sound approach. Because tremendous numerical efforts were needed to solve the integral equations in RRDA, the physics in this approach had only been studied for small coupling constants,[13] and there existed no solutions to RRDA from the intermediate- to strong-coupling regimes. To develop a numerical scheme to solve RRDA equations for the purpose of understanding 2DES in a wider range of couplings is still a challenging problem in modern many-particle physics.

In this paper, we use a superhigh-efficiency algorithm to solve the RRDA equations. With the solutions, the ground-state energy is obtained, and it is in excellent agreement with the result of the fixed-node-diffusion Monte Carlo (MC) simulation.[14] In addition, the self-energy of Green's function, the effective mass, the single-particle distribution function, as well as the renormalization factor of Green's function are also calculated.

II. FORMALISM

We consider a 2DES with density of n at temperature T embedded in a uniform neutralizing background of positive charge. Throughout this paper, we will use the units in which $\hbar = k_B = m = a = 1$ (with m the mass of the electron and a the Wigner-Seitz radius of an electron in the 2DES). The system is characterized by two dimensionless parameters:

$$\theta = T/E_F, \tag{1}$$

$$r_s = a/a_B, \tag{2}$$

where $E_F = \pi n$ (=1 in our units) is the Fermi energy and a_B the Bohr radius. The electronic Green's function G is related to the self-energy Σ via

$$G(\vec{k}, i\omega_n) = [i\omega_n - \xi_{\vec{k}} - \Sigma(\vec{k}, i\omega_n)]^{-1}, \tag{3}$$

where $\xi_k = \epsilon_k - \mu$ with $\epsilon_k = k^2/2$ and μ the chemical potential, and ω_n is the fermionic Matsubara frequency. For brevity, we hereafter will use $k \equiv (\vec{k}, i\omega_n)$ for the argument unless stated otherwise. By the RRDA which is shown in Fig. 1,[12] the self-energy Σ is given by

$$\Sigma(k) = -\frac{1}{V\beta}\sum_q G(k+q)\frac{V(q)}{1 - V(q)\chi(q)}, \tag{4}$$

where $\beta = 1/T$, $V(q) = 2\pi r_s/q$ is the Coulomb interaction, V is the area of the system, and

$$\chi(q) = \frac{2}{V\beta}\sum_k G(k)G(k+q) \tag{5}$$

is the electron polarizability, where $q \equiv (\vec{q}, i\Omega_m)$ with Ω_m the bosonic Matsubara frequency. The chemical potential μ is determined by the electron density,

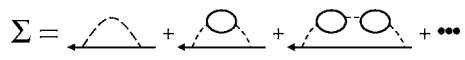

FIG. 1. Renormalized-ring-diagram approximation for the self-energy. The dashed line represents the Coulomb interaction. The bubbles are the electron polarizability in which the solid lines are the renormalized Green's functions.

$$n = \frac{2}{V\beta}\sum_k G(k)\exp(i\omega_n 0^+). \quad (6)$$

By solving Eqs. (3)–(6), the functions G and Σ and the chemical potential μ can be self-consistently obtained.

III. NUMERICAL ALGORITHM

In the numerical procedure, the most time-consuming computations are calculations of Σ and χ because of the summation over the Matsubara frequency and the integration over the momentum. We have developed an effective algorithm for doing such a computation. In this method, the summation is taken only over some selected Matsubara frequencies distributed in L successively connected blocks, each of them containing M frequencies, with each term under the summation multiplied by a weighting factor. For details of this algorithm, the reader is referred to Ref. 15. In the present calculation, we have used the parameters $[h,L,M]=[2,15,5]$ for selection of the Matsubara frequencies, where h is the integer parameter that the stride in the ℓth block is $h^{(\ell-1)}$. The total number of the selected frequencies is $L(M-1)+1=61$, with the largest number $N\sim 2^L(M-1)=2^{17}$ for the cutoff frequencies $\Omega_N=2N\pi T$ and $\omega_N=(2N-1)\pi T$. We will see later that the 61 Matsubara frequencies are sufficient to describe the self-energy and, thereby, Green's function. Instead of summing over N Matsubara frequencies by a usual method, we here take the summation only over the 61 ones. Therefore, the efficiency of the algorithm for the present calculation is $N/61\sim 2^{11}$! For the lowest temperature considered here, $\theta=0.03$, we have $\omega_N/E_F\sim 2.47\times 10^4$. In our calculation, the largest ϵ_k is $\epsilon_M=k_M^2/2$ with $k_M=50$. Therefore, the cutoff $\omega_N/\epsilon_M\sim 20$ is sufficiently large.

On the other hand, the momentum-space convolution integrals in Eqs. (4) and (5) can be easily performed by Fourier transforming into real space. For illustrating the two-dimensional Fourier transform, we here discuss the transformation of Green's function. In the real space, Green's function is given by

$$G(r,i\omega_n) = \int_0^\infty \frac{dk}{2\pi} kG(\vec{k},i\omega_n)J_0(kr), \quad (7)$$

where J_0 is the first kind Bessel function of order zero. However, Eq. (7) is not in a favorite form for the numerical computation since $kG(\vec{k},i\omega_n)$ behaves like $O(1/k)$ at $k\to\infty$ and $j_0(kr)$ is an oscillatory function; the integrand decreases so slowly at large k that a precise numerical result is hardly obtained. By observing the asymptotic behavior,

$$G(\vec{k},i\omega_n)\to G^0(\vec{k},i\omega_n) \quad \text{at } k\to\infty \text{ or } n\to\infty, \quad (8)$$

with $G^0(\vec{k},i\omega_n)=1/(i\omega_n+\mu_0-k^2/2)$ and $\mu_0=E_F+T\ln[1-\exp(-1/\theta)]$, respectively, Green's function and the chemical potential of the free electrons, we choose G^0 as the auxiliary function for G. The Fourier transform of $G^0(\vec{k},i\omega_n)$ is given by

$$G^0(r,i\omega_n) = -K_0(pr)/\pi, \quad (9)$$

where K_0 is the second kind modified Bessel function of order zero and $p=(-2\mu_0-i2\omega_n)^{1/2}$. Thus, Eq. (7) can be rewritten as

$$G(r,i\omega_n) = \int_0^\infty \frac{dk}{2\pi} k\delta G(\vec{k},i\omega_n)J_0(kr) - K_0(pr)/\pi, \quad (10)$$

with $\delta G(\vec{k},i\omega_n)=G(\vec{k},i\omega_n)-G^0(\vec{k},i\omega_n)$. Now, the integrand in Eq. (10) drops fastly with $k\delta G(\vec{k},i\omega_n)\sim O(k^{-3})$ at $k\to\infty$. Equation (10) can be further reformed for dealing with the fast oscillatory behavior of $J_0(kr)$ at large r. In the Appendix, our numerical method for such integration is detailed.

In the above example, the accuracy and efficiency of numerical integration are improved by choosing the proper auxiliary function. Analogously, we can choose the auxiliary function for the summation over the Matsubara frequency as well. For example, the auxiliary function for calculating $\chi(q)$ is chosen as $G^0(k)G^0(k+q)$, which is the asymptotic limit of $G(k)G(k+q)$ at $\omega_n\to\infty$ or $k\to\infty$. On the other hand, the free-particle polarizability $\chi^0(q)$ can be easily obtained by

$$\chi^0(\vec{q},i\Omega_m) = \frac{\beta}{4\pi}\int_0^\infty d\epsilon \frac{Y(q,\Omega_m)-1}{\cosh^2[(\epsilon-\mu_0)/2T]}, \quad (11)$$

with $Y(q,\Omega_m)=(\sqrt{x^2+y^2}+x)^{1/2}$, where $x=1/2-\Omega_m^2/2\epsilon_q^2-2\epsilon/\epsilon_q$ and $y=\Omega_m/\epsilon_q$. Similarly, we can deal with the exchange self-energy that is represented by the first diagram in Fig. 1. It can be written as

$$\Sigma_x(k) = -\frac{1}{V\beta}\sum_{k'}[G(k')-G^0(k')]V(|\vec{k}-\vec{k}'|)+\Sigma_x^0(k). \quad (12)$$

Here, $\Sigma_x^0(k)$ is the exchange self-energy of the nonrenormalized electrons,

$$\Sigma_x^0(k) = -\frac{2r_s}{\pi}\int_0^\infty dk' \frac{k'}{k+k'}F^0(k')K(\alpha), \quad (13)$$

where F^0 is the Fermi distribution function of the free electrons and $K(\alpha)$ is the complete elliptic integral of the first kind with $\alpha=2\sqrt{kk'}/(k+k')$. The function $K(\alpha)$ has a logarithmic singularity at $\alpha=1$, which can be eliminated by choosing the auxiliary function $-\frac{1}{2}F^0(k)\ln|k'-k|$ for the integrand within a finite range of k'.

IV. RESULTS

By iteration, we have solved Eqs. (3)–(6) for $0<r_s\leqslant 30$ at finite temperatures. Firstly, in order to illustrate the validity of our selection for the Matsubara frequencies, we show

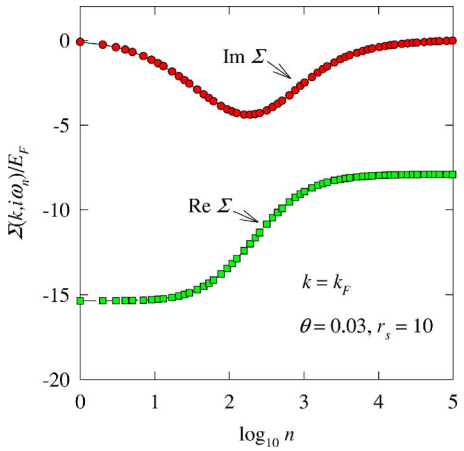

FIG. 2. (Color online) Self-energy $\Sigma(k, i\omega_n)$ as function of n at $k=k_F$, $\theta=0.03$, and $r_s=10$.

in Fig. 2 the result for the self-energy $\Sigma(\vec{k}, i\omega_n)$ for $k=k_F$, $\theta=0.03$, and $r_s=10$. The symbols represent the values of $\Sigma(\vec{k}, i\omega_n)$ calculated at the selected n's. This is a typical result of $\Sigma(k, i\omega_n)$ in the strong-coupling regime. As seen in Fig. 2, the selected frequencies are sufficient for describing $\Sigma(\vec{k}, i\omega_n)$; though the selected ω_n's are sparsely distributed at large n, meanwhile, the function $\Sigma(\vec{k}, i\omega_n)$ varies slowly. At $\omega_n \to \infty$, the imaginary part of $\Sigma(k, i\omega_n)$ vanishes, but the real part remains finite. Actually, at $\omega_n \to \infty$, we get $\Sigma(\vec{k}, i\omega_n) \to$ the exchange part of the self-energy.

With the result for Green's function, we calculate the physical quantities of the system. The energy per electron is defined by

$$\epsilon = \frac{1}{N}\sum_{\vec{k}} [2\epsilon_k + \Sigma_x(k)]n(k) - \frac{1}{2\beta N}\sum_q \frac{V^2(q)\chi^2(q)}{1 - V(q)\chi(q)}, \tag{14}$$

where $N=nV$ is the total number of the electrons and $n(k)$ is the distribution function defined by

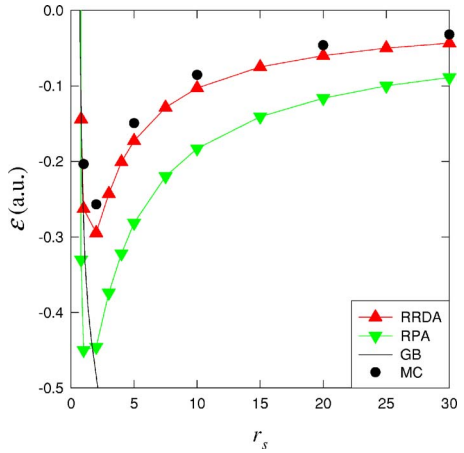

FIG. 3. (Color online) Ground-state energy as function of r_s. The present result (RRDA) is compared with that of the RPA, GB (Ref. 3), and MC (Ref. 14).

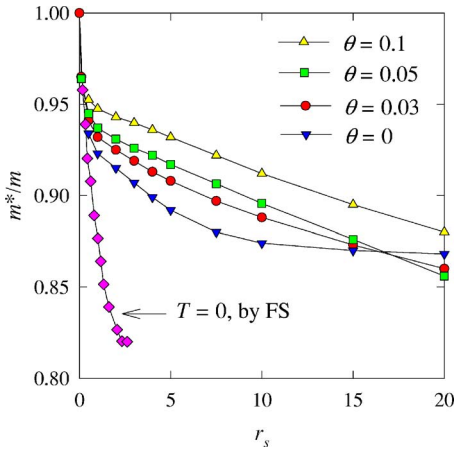

FIG. 4. (Color online) Effective mass m^*/m as function of r_s at $\theta=0$, 0.03, 0.05, and 0.1. The present results are compared with that of Ref. 13 (FS) at $T=0$ obtained with a different numerical method.

$$n(k) = \frac{1}{\beta}\sum_n G(\vec{k}, i\omega_n)\exp(i\omega_n 0^+). \tag{15}$$

In Fig. 3, the ground-state energy per electron in atomic unit is shown as a function of r_s. The results of the present calculation are obtained by extrapolation of the finite-temperature values. Our main result denoted by RRDA is compared with the RPA, the high-density expansion[3] by the scheme of Gell-Mann and Brueckner (GB),[16] and the variational MC simulation.[14] In the weak-coupling regime, both the RRDA and RPA reproduce the GB result very well. However, for strong coupling, the RRDA is much closer to the MC than the RPA. The MC data are believed to be the most reliable result for the ground-state energy. Therefore, the RRDA seems much better than the RPA.

We next consider the effective mass m^*/m,

$$m^*/m = \frac{1 - \left.\frac{\partial}{\partial E}\mathrm{Re}\,\Sigma_r(k_F, E)\right|_{E=0}}{1 + \left.\frac{\partial}{k_F \partial k}\mathrm{Re}\,\Sigma_r(k, 0)\right|_{k=k_F}}, \tag{16}$$

where $\Sigma_r(k, E)$ is the analytical continuation of $\Sigma(k, i\omega_n)$ under $i\omega_n \to E + i0^+$. Our result for $\Sigma_r(k, E)$ is obtained by the Padé approximation.[17] Shown in Fig. 4 is the effective mass m^*/m as a function of r_s at $\theta=0$, 0.03, 0.05, and 0.1. The values for $\theta=0$ are obtained by extrapolations from the finite-temperature results. The results of Faleev and Stockman (FS) calculated with a different numerical scheme for $T=0$ are also depicted for comparison. [We find that m^*/m very sensitively depends on $d\Sigma(k,0)/dk|_{k=k_F}$. The discrepancy between the present and FS results may be due to some numerical errors in the latter.] The present results show that m^*/m is a monotonically decreasing function of r_s in a wide range of r_s at low temperatures. This is different from the RPA (not shown here), by which the ground-state quantity m^*/m decreases at small $r_s \leqslant 0.1$, but then increases with r_s.[5]

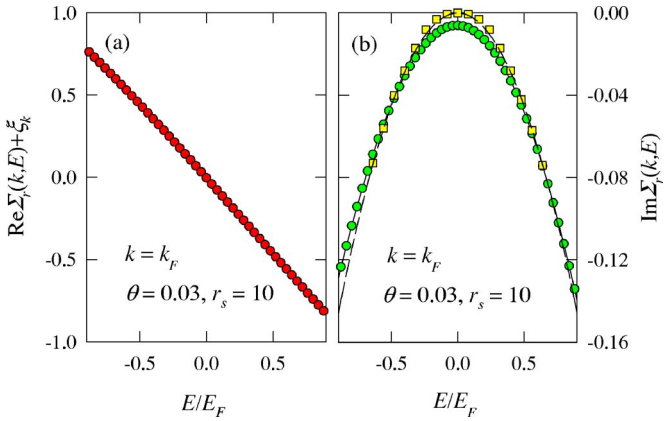

FIG. 5. (Color online) Self-energy $\Sigma_r(k,E)$ as function of E at $k=k_F$ for $\theta=0.03$ and $r_s=10$. (a) $\mathrm{Re}\,\Sigma_r(k_F,E)+\xi_{k_F}$ and (b) the imaginary part. The squares in (b) are obtained by extrapolations to $\theta=0$. The dashed line is a plot of $-0.18E^2$. For the real part, the extrapolated results are indistinguishable from the line in (a).

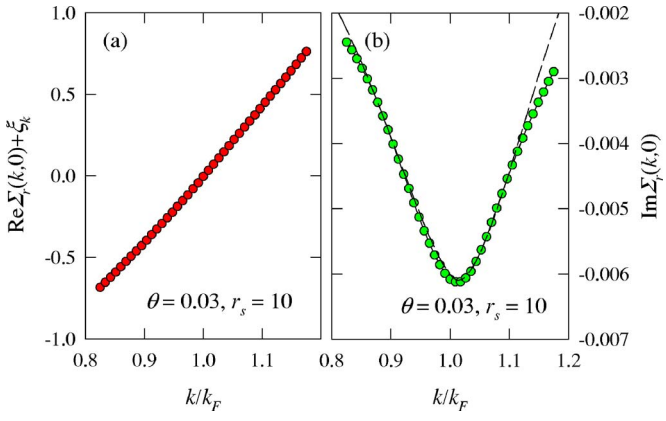

FIG. 6. (Color online) Self-energy $\Sigma_r(k,0)$ as function of k at $\theta=0.03$ and $r_s=10$. (a) $\mathrm{Re}\,\Sigma_r(k,0)+\xi_k$ and (b) imaginary part. The dashed line represents the function given by Eq. (17).

The present results on m^*/m seem to be contradictory to the explanation to the experiments on the temperature dependence of the Shubnikov–de Haas oscillations in a 2DES.[18] The experiments were explained as m^*/m increasing with r_s. To this point, there may be two possibilities: (1) the RRDA may not be good enough or (2) the experimental results may require a different interpretation; for example, the conductivity formula to fit the experiments was based on noninteracting electrons except that the mass is assumed to be renormalized. Further investigation is needed to get a clear understanding of this problem.

The effective mass m^*/m has been extensively investigated by many calculations using the RPA. With the RPA self-energy, m^*/m is calculated by the on-shell scheme,[2] which is not a self-consistent approximation for the quasiparticle energy. Contrary to the RPA, the RRDA is a conserving approximation for the single-particle Green's function;[12] Green's function satisfies the Luttinger theorem,[19,20] by which the Fermi surface is unchanged for the 2DES. To see this, we show in Fig. 5 the retarded self-energy $\Sigma_r(k,E)$ as function of E at $k=k_F$ for $\theta=0.03$ and $r_s=10$. $\mathrm{Re}\,\Sigma_r(k_F,E)$ is essentially a linear function of E in the neighborhood of $E=0$. It is clear that $\mathrm{Re}\,\Sigma_r(k_F,0)+\xi_{k_F}=0$, which means that the quasiparticle energy E vanishes at the Fermi surface, consistent with the Luttinger theorem. The equality $\mathrm{Re}\,\Sigma_r(k_F,0)+\xi_{k_F}=0$ originates from the fact that $\mathrm{Re}\,\Sigma_r(k_F,0)$ is compensated by the shift of the renormalized μ from μ_0. The imaginary part shown in Fig. 5(b) has a parabola form with a small value at $E=0$. At $T=0$, $\mathrm{Im}\,\Sigma_r(k_F,E)\propto -E^2$ at small E.[19] The small negative value of $\mathrm{Im}\,\Sigma_r(k_F,0)$ shown in Fig. 5(b) is a finite-temperature effect. The squares in Fig. 5(b) are obtained by extrapolations to $\theta=0$ from the finite-temperature results. The dashed line is given by $-0.18E^2$, which shows that $\mathrm{Im}\,\Sigma_r(k_F,E)$ is indeed a quadratic form at small E. For the real part, the extrapolated results are indistinguishable from the line in Fig. 5(a). (All these facts indicate that our numerical computation is very accurately performed.) On the other hand, since the bare chemical potential μ_0 is used in the RPA calculation, $\mathrm{Re}\,\Sigma_r(k_F,0)$ cannot be compensated and, thereby, the quasiparticle energy does not vanish at k_F.

It should be pointed out here that our result for $\mathrm{Im}\,\Sigma_r(k_F,E)$ is different from that of the RPA. By RPA, the zero-temperature result is $\mathrm{Im}\,\Sigma_r(k_F,E)\propto E^2\ln(|E|)$ at small E.[21,22] However, by RRDA, there is no additional logarithmic factor.

In Fig. 6, the zero-frequency self-energy $\Sigma_r(k,0)$ at $\theta=0.03$ and $r_s=10$ is shown as a function of k. The real part is a linear function of k around k_F with a positive slope. The magnitude of the imaginary part is very small. The largest magnitude appears at k_F, which corresponds to the small negative value that appeared in Fig. 5(b) at $E=0$. The dashed line in Fig. 5(b) is a plot of the function

$$\Gamma(k) = -0.03\tilde{\xi}_k^2 \ln(|\tilde{\xi}_k|) - 0.0061, \tag{17}$$

with $\tilde{\xi}_k=(k/k_F)^2-1.03$. This function fits very well to $\mathrm{Im}\,\Sigma_r(k,0)$ at wave number k close to k_F.

In Fig. 7, we exhibit the result for the distribution function $n(k)$ at $\theta=0.03$ for various r_s. It is well known that $n(k)$ at $r_s=0$ is the Fermi-Dirac distribution function $F^0(k)$ for the free electrons. At very small r_s, $n(k)$ is close to $F^0(k)$. With increasing r_s, $n(k)$ becomes very different from $F^0(k)$; it is gradually suppressed at $k<k_F$, while it increases at $k>k_F$. At the Fermi momentum, $n(k)$ decreases dramatically, but seems continuous. At zero temperature, $n(k)$ should have a discontinuity at $k=k_F$. For $r_s=10$, the extrapolated results at $T=0$ are shown in Fig. 7. As seen, the ground-state values are very close to the curve at $\theta=0.03$. The continuous behavior that appeared in Fig. 7 is attributed to the finite-temperature effect by which the discontinuity is rounded. At zero temperature, the magnitude of the abrupt drop in $n(k)$ at k_F is associated with the renormalization factor Z of Green's function. This factor is defined by

$$Z = \left[1 - \frac{\partial}{\partial E}\,\mathrm{Re}\,\Sigma_r(k_F,E)\big|_{E=0}\right]^{-1}. \tag{18}$$

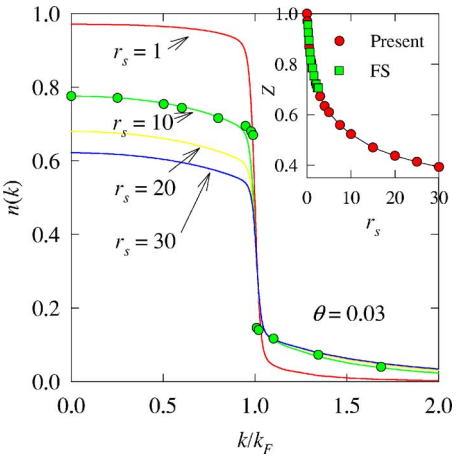

FIG. 7. (Color online) Distribution function $n(k)$ at $\theta=0.03$ and various r_s. The circles are the extrapolated results at $T=0$ for $r_s=10$. The inset is the Z factor as function of r_s. The circles in the inset represent the results of the present calculation, and the squares are that of Ref. 13.

Shown in the inset of Fig. 7 is the renormalization factor Z. Within the range of r_s studied here, the magnitude of Z is consistent with the sharp drop in $n(k)$ at k_F. For comparison, the result by FS is also shown in the inset. By their method,[13] they could solve the RRDA equations only within $r_s \leqslant 2.62$. Clearly, their result is reproduced by the present calculation.

V. SUMMARY

In summary, we have solved the RRDA equations for 2DES at $r_s \leqslant 30$ with our superhigh-efficiency numerical algorithm. The obtained ground-state energy is in excellent agreement with the Monte Carlo result. For the effective mass m^*/m, the RRDA result shows that m^*/m is a decreasing function of r_s, which is considerably different from the RPA. The distribution function $n(k)$ and the renormalization factor Z of Green's function are calculated for a wide range of r_s. The renormalization factor Z obtained by the present calculation is consistent with the discontinuity in the distribution function at the Fermi momentum at zero temperature.

ACKNOWLEDGMENTS

The authors thank Q. Wang for useful discussion on the related problems. This work was supported by a grant from the Robert A. Welch Foundation under No. E-1146, the TCSUH, and the National Basic Research 973 Program of China under Grant No. 2005CB623602.

APPENDIX

In this appendix, we deal with the integral

$$g(r) = \int_0^\infty dk f(k) J_0(kr), \tag{A1}$$

which appeared in the Fourier transform of a two-dimensional function. At large r, since $J_0(kr)$ is a fast oscillatory function, the integral cannot be precisely computed by simple numerical integration. By observing the asymptotic behavior of $J_0(z)$ at $z \to \infty$,

$$J_0(z) \sim \frac{1}{\sqrt{\pi z}}\left[\sin z + \cos z + \frac{1}{8z}(\sin z - \cos z)\right],$$

we choose the auxiliary function as

$$A(kr) = \sqrt{\frac{c}{kr+c}}\left\{\sin(kr) + \cos(kr) + \frac{kr}{8(kr+c)^2}[\sin(kr) - \cos(kr)]\right\},$$

with $c = 1/\pi$. $A(kr)$ has the same asymptotic behavior as $J_0(kr)$ at $k \to \infty$ or $r \to \infty$. In addition, $A(0) = J_0(0) = 1$. With this auxiliary function, Eq. (A1) can be rewritten as

$$g(r) = \int_0^\infty dk f(k)[J_0(kr) - A(kr)] + \sqrt{c}\int_0^\infty dk \frac{f(k)}{\sqrt{kr+c}}\left[1 - \frac{kr}{8(kr+c)^2}\right]\cos(kr) + \sqrt{c}\int_0^\infty dk \frac{f(k)}{\sqrt{kr+c}}\left[1 + \frac{kr}{8(kr+c)^2}\right]\sin(kr).$$

Now, the first integral in the above equation can be integrated by the simple numerical method since the fast oscillatory behavior of J_0 is considerably canceled by $A(kr)$. On the other hand, the second and third Fourier integrals can be numerically integrated using Filon's method. In our numerical calculation, the momentum integration is over the range $0 \leqslant k \leqslant 50$. Because the electron distribution function varies drastically around the Fermi momentum, we divide the k range into three segments: $[0, k_F - k_0]$, $[k_F - k_0, k_F + k_0]$, and $[k_F + k_0, 50]$, where $k_F = \sqrt{2}$ and $k_0 = \sqrt{8\theta}/(1 + \sqrt{32\theta})$. The k integrals are calculated with 200 meshes in each segment. In the real space, r is confined to $0 \leqslant r \leqslant 80$, which is divided into three segments: [0,5], [5,30], and [30,80], with 300 meshes in each segment.

[1] T. Ando, A. B. Fowler, and F. Stern, Rev. Mod. Phys. **54**, 437 (1982).
[2] C. S. Ting, T. K. Lee, and J. J. Quinn, Phys. Rev. Lett. **34**, 870 (1975).
[3] A. K. Rajagopal and J. C. Kimball, Phys. Rev. B **15**, 2819 (1977).
[4] Ben Yu-Kuang Hu, Phys. Rev. B **47**, 1687 (1993); Ben Yu-Kuang Hu and S. Das Sarma, *ibid.* **48**, 5469 (1993).
[5] S. Das Sarma, V. M. Galitski, and Y. Zhang, Phys. Rev. B **69**, 125334 (2004).

[6] K. S. Singwi, M. P. Tosi, R. H. Land, and A. Sjölander, Phys. Rev. **176**, 589 (1968).
[7] K. Utsumi and S. Ichimaru, Phys. Rev. A **26**, 603 (1982).
[8] N. Iwamoto, Phys. Rev. B **43**, 2174 (1991).
[9] Y.-R. Jang and B. I. Min, Phys. Rev. B **48**, 1914 (1993).
[10] S. Yarlagadda and G. F. Giuliani, Phys. Rev. B **49**, 14188 (1994).
[11] G.-H. Chen and M. E. Raikh, Phys. Rev. B **60**, 4826 (1999).
[12] G. Baym and L. P. Kadanoff, Phys. Rev. **124**, 287 (1961); G. Baym, *ibid.* **127**, 1391 (1962).
[13] S. V. Faleev and M. I. Stockman, Phys. Rev. B **62**, 16707 (2000); **63**, 193302 (2001).
[14] C. Attaccalite, S. Moroni, P. Gori-Giorgi, and G. B. Bachelet, Phys. Rev. Lett. **88**, 256601 (2002); **91**, 109902(E) (2003).
[15] X.-Z. Yan, Phys. Rev. B **71**, 104520 (2005).
[16] M. Gell-Mann and K. A. Brueckner, Phys. Rev. **106**, 364 (1957).
[17] H. J. Vidberg and J. W. Serene, J. Low Temp. Phys. **29**, 179 (1977).
[18] A. A. Shashkin, M. Rahimi, S. Anissimova, S. V. Kravchenko, V. T. Dolgopolov, and T. M. Klapwijk, Phys. Rev. Lett. **91**, 046403 (2003); A. A. Shashkin, S. V. Kravchenko, V. T. Dolgopolov, and T. M. Klapwijk, Phys. Rev. B **66**, 073303 (2002).
[19] J. M. Luttinger and J. C. Ward, Phys. Rev. **118**, 1417 (1960).
[20] J. M. Luttinger, Phys. Rev. **119**, 1153 (1960).
[21] T. Jungwirth and A. H. MacDonald, Phys. Rev. B **53**, 7403 (1996).
[22] L. Zheng and S. Das Sarma, Phys. Rev. B **53**, 9964 (1996).